NASA/TM-20205009287

Residual Stresses Induced Due to Curing of the Bulk Matrix in a Simplified Three-Dimensional (3D) Woven Repeating Unit Cell

Kalima Bukenya, Michael Olaya, and Sagar Shah
University of Massachusetts Lowell, Lowell, Massachusetts

Evan J. Pineda and Trenton M. Ricks
Glenn Research Center, Cleveland, Ohio

Marianna Maiarù
University of Massachusetts Lowell, Lowell, Massachusetts

August 2021

NASA STI Program . . . in Profile

Since its founding, NASA has been dedicated to the advancement of aeronautics and space science. The NASA Scientific and Technical Information (STI) Program plays a key part in helping NASA maintain this important role.

The NASA STI Program operates under the auspices of the Agency Chief Information Officer. It collects, organizes, provides for archiving, and disseminates NASA's STI. The NASA STI Program provides access to the NASA Technical Report Server—Registered (NTRS Reg) and NASA Technical Report Server—Public (NTRS) thus providing one of the largest collections of aeronautical and space science STI in the world. Results are published in both non-NASA channels and by NASA in the NASA STI Report Series, which includes the following report types:

- TECHNICAL PUBLICATION. Reports of completed research or a major significant phase of research that present the results of NASA programs and include extensive data or theoretical analysis. Includes compilations of significant scientific and technical data and information deemed to be of continuing reference value. NASA counter-part of peer-reviewed formal professional papers, but has less stringent limitations on manuscript length and extent of graphic presentations.

- TECHNICAL MEMORANDUM. Scientific and technical findings that are preliminary or of specialized interest, e.g., "quick-release" reports, working papers, and bibliographies that contain minimal annotation. Does not contain extensive analysis.

- CONTRACTOR REPORT. Scientific and technical findings by NASA-sponsored contractors and grantees.

- CONFERENCE PUBLICATION. Collected papers from scientific and technical conferences, symposia, seminars, or other meetings sponsored or co-sponsored by NASA.

- SPECIAL PUBLICATION. Scientific, technical, or historical information from NASA programs, projects, and missions, often concerned with subjects having substantial public interest.

- TECHNICAL TRANSLATION. English-language translations of foreign scientific and technical material pertinent to NASA's mission.

For more information about the NASA STI program, see the following:

- Access the NASA STI program home page at http://www.sti.nasa.gov

- E-mail your question to help@sti.nasa.gov

- Fax your question to the NASA STI Information Desk at 757-864-6500

- Telephone the NASA STI Information Desk at 757-864-9658

- Write to:
  NASA STI Program
  Mail Stop 148
  NASA Langley Research Center
  Hampton, VA 23681-2199

NASA/TM-20205009287

Residual Stresses Induced Due to Curing of the Bulk Matrix in a Simplified Three-Dimensional (3D) Woven Repeating Unit Cell

Kalima Bukenya, Michael Olaya, and Sagar Shah
University of Massachusetts Lowell, Lowell, Massachusetts

Evan J. Pineda and Trenton M. Ricks
Glenn Research Center, Cleveland, Ohio

Marianna Maiarù
University of Massachusetts Lowell, Lowell, Massachusetts

National Aeronautics and
Space Administration

Glenn Research Center
Cleveland, Ohio 44135

August 2021

Acknowledgments

This work was funded by NASA's Composite Technology for Exploration (CTE) Project in part through a Lewis' Educational and Research Collaborative Internship Project (LERCIP) internship.

Level of Review: This material has been technically reviewed by technical management.

Available from

NASA STI Program
Mail Stop 148
NASA Langley Research Center
Hampton, VA 23681-2199

National Technical Information Service
5285 Port Royal Road
Springfield, VA 22161
703-605-6000

This report is available in electronic form at http://www.sti.nasa.gov/ and http://ntrs.nasa.gov/

Residual Stresses Induced Due to Curing of the Bulk Matrix in a Simplified Three-Dimensional (3D) Woven Repeating Unit Cell

Kalima Bukenya,* Michael Olaya, and Sagar Shah
University of Massachusetts Lowell
Lowell, Massachusetts 01854

Evan J. Pineda and Trenton M. Ricks
National Aeronautics and Space Administration
Glenn Research Center
Cleveland, Ohio 44135

Marianna Maiarù
University of Massachusetts Lowell
Lowell, Massachusetts 01854

Abstract

It has been observed that 3D woven materials are highly susceptible to processes induced defects including tow misalignment, intratow and intertow cracking and/or voids. Adequate process modeling of 3D woven Polymer Matrix Composites (PMCs) is necessary to predict and estimate the effects of the manufacturing process on these defects. A preliminary step towards this is achieved with the commercial Finite Element Analysis (FEA) tool Abaqus complemented with written user subroutines to account for the effect of shrinkage and thermoelastic properties evolution as a function of the degree of cure of the bulk matrix phase in a 3D woven composite repeating unit cell (RUC). As a pathfinder, the process modeling framework is demonstrated on a simplified 3D woven RUC of an AS4/RIMR 135 system. Curing simulations are performed on the 3D woven RUC to observe the processing induced residual stresses. The results of the analysis show that high stress concentrations, present within the 3D intertow matrix bordering the binder tow, coincide with X-Ray computed tomography (X-Ray-CT) scan data depicting cracking in the same location.

1.0 Introduction

Two-dimensional (2D) carbon fiber polymer matrix composites (PMCs) are widely used for aerospace structural applications (Refs. 1 and 2). While they maintain their lightweight and high strength characteristics, 2D PMCs have weaker out-of-plane properties and are therefore susceptible to delamination failure (Ref. 3). Three-dimensional (3D) woven PMCs typically contain perpendicular warp and weft tows that are stacked and woven together using a binder tow through the thickness of the composite and increasing its out-of-plane strength. These strength improvements achieved with 3D PMCs make them viable materials for aerospace applications where through thickness stresses may be high (Refs. 4 to 8). However, it has been observed that 3D woven materials are highly susceptible to processes induced defects such as tow misalignment, as well as intratow and intertow cracking and/or voids (Refs. 9 to 11).

*Intern in Lewis' Educational and Research Collaborative Internship Project (LeRCIP).

Process modeling of PMCs can be used to understand the effects of manufacturing on the formation of defects and the consequential performance of the structure (Refs. 12 to 17). High fidelity virtual testing is conducted at the microscale where the effective constitutive properties of the composite material are homogenized such that predictions can be made at higher length scales. While process modeling techniques have been extensively explored with traditional unidirectional PMCs, very little work has been done to apply this method to 3D woven PMCs. Wang et al. created a multiscale process modeling approach for a 3D woven PMC with a cure-hardening instantaneous linear elastic (CHILE) model to predict the residual defects (Ref. 18). Tsukrov et al. employed microscale numerical modeling techniques to create realistic finite element models of 3D woven composites and applied a thermal cooldown to predict the cure-induced stresses within the microstructure and validate the results with micro-computed tomography (Micro-CT) scans (Ref. 19). A numerical modeling method was proposed in complemented with blind hole drilling experiments by Vasylevskyi et al. to observe and quantify process-induced stresses in mesoscale finite element (FE) models during a thermal cooling process (Ref. 20). Gross et al. modified cure cycle profiles to mitigate the hydrostatic tensile stresses induced by a mismatch in constituent thermal properties during the thermal cooling of a 3D woven composite (Ref. 21).

A CHILE model proposed by Maiarù et al. is used in this study to calculate process-induced defects in 3D woven PMCs (Refs. 22 and 23). Residual stresses in the intertow matrix are characterized with respect to time, temperature, and degree of cure for a one-hold cure cycle. Cure kinetics are calculated from the Arrhenius model. The commercial finite element analysis (FEA) software Abaqus is used to solve the heat equation. Written UMATHT and UMAT user-subroutines are coupled with the software to account for contributions made by the resin exotherm. The 3D woven geometry contains a single binder tow surrounded by bulk matrix. Hexahedral mesh elements are used in the tow while a tetrahedral mesh is imposed on the bulk matrix to ensure convergence. An AS4/RIMR135 material system is chosen for this study. Properties for RIMR135 resin are characterized experimentally while AS4 properties were found in literature. Thermomechanical properties for the composite system are approximated using the Rule of Mixtures (ROM) and Bridging Model. Virtual testing is conducted in Abaqus with the cure kinetics applied only to the bulk matrix with user-defined material inputs. The tow properties during cure remain linear elastic with Abaqus-defined material inputs. Results from this model are then compared with existing Micro-CT scan data depicting cracking within 3D woven PMCs.

This manuscript is outlined as follows. Section 2.0 will deliver the project methodology which includes the theory and analysis approach. Section 3.0 will describe the modelling details and material parameters. Section 4.0 will provide an overlay of the results with some discussion. Section 5.0 will summarize the findings and identify contributions to future work.

2.0 Project Methodology

2.1 Theory

The CHILE approach is used to predict the process-induced stresses during a simple single-hold cure cycle (Ref. 24).

2.1.1 Constitutive Model

The CHILE model assumes an instantaneous linear elastic material with a constant stiffness for each time step. The evolution of stress $\sigma_i(t)$ as a function of time t can be defined as:

$$\sigma_i(t) = \left[C_{ij}(t)\right]\left[\varepsilon_j^t(t) - \left(\varepsilon_j^{th}(t) + \varepsilon_j^c(t)\right)\right] \tag{1}$$

where ε^t is the total strain, ε^{th} is the thermal strain, and ε^c is the chemical shrinkage. $C_{ij}(t)$ is the six-by-six stiffness matrix for an isotropic material that defines instantaneous mechanical properties for a given time during the curing process:

$$C_{ij}(t) = \frac{E(t)}{(1+\nu(t))(1-2\nu(t))}\begin{bmatrix} 1-\nu(t) & \nu(t) & \nu(t) & 0 & 0 & 0 \\ \nu(t) & 1-\nu(t) & \nu(t) & 0 & 0 & 0 \\ \nu(t) & \nu(t) & 1-\nu(t) & 0 & 0 & 0 \\ 0 & 0 & 0 & 1-2\nu(t) & 0 & 0 \\ 0 & 0 & 0 & 0 & 1-2\nu(t) & 0 \\ 0 & 0 & 0 & 0 & 0 & 1-2\nu(t) \end{bmatrix} \quad (2)$$

$E(t)$ and $\nu(t)$ respectively represent the time-dependent Young's modulus and Poisson's ratio of the matrix.

2.1.2 Heat Transfer Equation

As the resin-system cures, heat is transferred through conduction. As the curing of thermoset composites is an exothermic reaction, there is also nonlinear internal heat generation. The transient heat transfer model used in this study is based on Fourier's equation for heat conduction (Ref. 26):

$$\rho^c c_p^c \frac{\partial T}{\partial t} = k_x^c \frac{\partial^2 T}{\partial x^2} + k_y^c \frac{\partial^2 T}{\partial y^2} + k_z^c \frac{\partial^2 T}{\partial z^2} + \frac{\partial H}{\partial t} \quad (3)$$

where H describes the internal enthalpic heat source. ρ^c and c_p^c are the composite density and specific heat. k^c is subscripted by x, y, and z to represent the anisotropic thermal conductivities in the material x-, y-, and z-directions. The material system used in this study is transversely orthotropic, and thus $k_y^c = k_z^c$.

2.1.3 Cure Kinetics

The rate of reaction, $\frac{d\phi}{dt}$ is directly proportional to the rate of heat flow, $\frac{dH}{dt}$. This is expressed mathematically below in Equation (4).

$$\frac{d\phi}{dt} = \frac{1}{H_T}\frac{dH}{dt} \quad (4)$$

The degree of cure, ϕ the calculated area under the curve of $\frac{d\phi}{dt}$ as a with respect to time t, as shown in Equation (5):

$$\phi = \frac{1}{H_T}\int_0^t \frac{dH}{dt}dt = \frac{H_{pr}}{H_T} \quad (5)$$

where H_{pr} represents the partial heat discharged for a given time t.

A semi-empirical expression proposed by Kamal (Ref. 27), which employs Arrhenius terms to the cure kinetics model, expands upon the heat equation to assert the direct proportionality between the rate of reaction and the degree of cure, shown in Equation (6).

$$\frac{d\phi}{dt} = (K_1 + K_2\phi^m)(1-\phi^n) \quad (6)$$

K_1 and K_2 are the Arrhenius temperature-dependent rate reactions with exponent constants m and n. The reaction rates can be calculated using Equation (7), which introduces dependent, frequency-like constants A_1 and A_2 and their respective activation energies ΔE_{a1} and ΔE_{a2} as a function of absolute temperature T:

$$K_i = A_i \exp\left(-\frac{\Delta E_{ai}}{RT}\right) \quad i = 1, 2 \tag{7}$$

where R represents the universal gas constant 8.3145 $\frac{\text{J}}{\text{mol·K}}$. The RIMR system used for this work was characterized using digital scanning calorimetry and thermogravimetric analysis. For simplicity and under isothermal considerations, the Prout-Thompkins model was used, and thus $A_2 = \Delta E_{a1} = 0$.

The cure kinetics model for the RIMR resin-system were determined experimentally from Differential Scanning Calorimetry (DSC) and Thermogravimetric Analysis (TGA). Cure kinetics parameters were then derived using the theory outlined above. These constants can be found in Section 3.1.

2.2 Homogenization of Thermal Properties

The density and effective thermal properties for AS4/RIMR135 were calculated using the Rule of Mixtures (ROM) approximation. Effective density is calculated with the following equation:

$$\rho^c = V^f \rho^f + \left(1 - V^f\right)\rho^m \tag{8}$$

Here, ρ^c is the effective density of the composite as a combined contribution of the fiber density ρ^f, the matrix density ρ^m, and dependent on the fiber volume fraction V^f. The specific heat capacity for the composite, c_p^c, was approximated with:

$$c_p^c = \frac{V^f \rho^f c_p^f + \left(1 - V^f\right)\rho^m c_p^m}{\rho^c} \tag{9}$$

where c_p^f and c_p^m represent the specific heat capacity of the fiber and the matrix, respectively. The composite longitudinal thermal conductivity k_A^c was found using the following relation:

$$k_A^c = V^f k_A^f + \left(1 - V^f\right)k^m \tag{10}$$

in which k_A^f is the longitudinal thermal conductivity of the fiber constituent while k^m is the thermal conductivity of the matrix material. Transverse thermal conductivities k_T^c for the composite were defined by:

$$k_T^c = k^m \left[\frac{k_T^f + 2k^m - 2V^f\left(k^m - k_T^f\right)}{k_T^f + 2k^m + V^f\left(k^m - k_T^f\right)}\right] \tag{11}$$

2.3 Analysis Approach

This work focuses mainly on the analysis approaches at the mesoscale, as shown below in Figure 1. First, there is a virtual curing test during which the cure kinetics are applied only to the intertow (bulk) matrix of the model using user-defined material properties. The tows at this stage maintain linear elastic constant material properties. The next step is a virtual curing test of the intratow matrix where the cure kinetics are applied to the tow weave using a homogenization approach. The intertow matrix maintains constant material properties. The final step is a combined virtual curing test of both the intertow and intratow matrix whereby the cure kinetics are coupled with both the tow and bulk matrix materials.

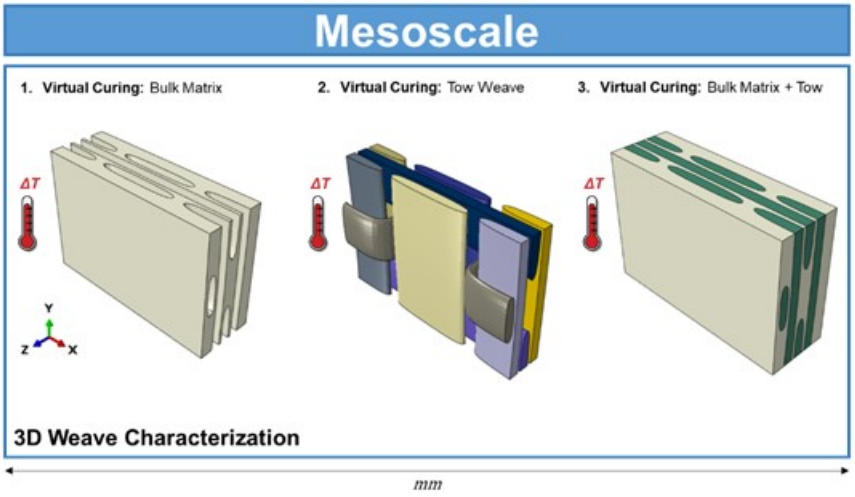

Figure 1.—Mesoscale Analysis Approach for a 3D Woven PMC.

The work discussed only covers up through Step 1 at the mesoscale, but intratow and cooperative intertow-intratow process-induced stresses will be analyzed in future work.

3.0 Model Parameters

3.1 Material Properties

The kinetic constants for the RIMR resin-system are listed below in Table 1. Additionally, the thermomechanical properties for the fiber and matrix material are shown in Table 2.

The density and thermal properties for the composite tow were approximated with Rule of Mixtures (ROM) as described in Section 3.2 and an assumed fiber volume fraction of 80 percent. Approximated density and thermal properties for the AS4/RIMR135 tow are shown in Table 3.

The matrix and fiber properties were homogenized using the Bridging Model to characterize the material parameters of the tow, presented in Table 4, with an 80 percent fiber volume faction (Ref. 28). FEA modeling allowed for these tow parameters to be obtained as a function of the fiber volume fraction, V^f, and degree of cure, ϕ.

3.2 Mesoscale Geometry

The 3D woven RUC of dimension (3.016 × 1.442 × 4.468) mm^3, containing elliptical warp/weft tows of (1.955 × 0.218) mm^2 and a (1.00 × 0.218) mm^2 elliptical binder tow was generated in Abaqus using a preexisting parametric script created by NASA (Ref. 29). This script allows the user to explore different tow geometries and mesh densities quickly. The geometry and mesh of the RUC are shown in Figure 2. The proposed configuration was chosen such that the computational analysis time may be minimized for this pathfinder study. While the geometry does not exactly represent the architecture of typical 3D woven specimens, the presence of warp, weft, and binder tows in this current model serve as a sufficient first step in analyzing the effects of the curing process at this scale. A coarse mesh of 0.1 mm was chosen to decrease computational time on the preliminary cure analyses. The tows have an 8-node trilinear displacement and temperature (C3D8T) hexahedral mesh. The bulk matrix utilized full integration 4-node thermal coupled tetrahedral elements (C3D4T) to avoid an unreasonably dense mesh.

TABLE 1.—KINETIC CONSTANTS FOR RIMR 135/RIMH 1366

Property		Unit	Value
Exponents	m	[-]	0.3
	n	[-]	1.5
Rate Constant	A_1	$[\mathrm{sec}^{-1}]$	11000
Activation Energy	ΔE_{a1}	[kJ/mol]	46.7

TABLE 2.—THERMOMECHANICAL MATERIAL PROPERTIES FOR RIMR 135 AND AS4 CARBON FIBER

Material	Property	Unit	Value
RIMR 135	E	2.50	[GPa]
	ν	0.37	[-]
	k	0.245	$\left[\frac{\mathrm{mW}}{\mathrm{mm}\cdot ^\circ\mathrm{C}}\right]$
	c_p	1.60E+09	$\left[\frac{\mathrm{mJ}}{\mathrm{tonnes}\cdot ^\circ\mathrm{C}}\right]$
	ρ	1.20E-09	$\left[\frac{\mathrm{tonnes}}{\mathrm{mm}^3}\right]$
	T_{cure}	80	[°C]
	T_{Room}	20	[°C]
	t_{cure}	34200	[s]
	ϕ_{gel}	0.82	[-]
Material	**Property**	**Value**	**Unit**
AS4	E_A	231	[GPa]
	E_T	15	[GPa]
	ν_{12}	0.21	[-]
	ν_{23}	0.30	[-]
	G_{12}	15.8	[GPa]
	G_{23}	5.77	[GPa]
	α_A	-0.5	$\left[10^{-6}/_{^\circ\mathrm{C}}\right]$
	α_T	15	$\left[10^{-6}/_{^\circ\mathrm{C}}\right]$
	k_A	6.83	$\left[\frac{\mathrm{mW}}{\mathrm{mm}\cdot ^\circ\mathrm{C}}\right]$
	k_T	0.1366	$\left[\frac{\mathrm{mW}}{\mathrm{mm}\cdot ^\circ\mathrm{C}}\right]$
	c_p	1.13E+09	$\left[\frac{\mathrm{mJ}}{\mathrm{tonnes}\cdot ^\circ\mathrm{C}}\right]$
	ρ	1.79E-09	$\left[\frac{\mathrm{tonnes}}{\mathrm{mm}^3}\right]$

TABLE 3.—DENSITY AND THERMAL PROPERTIES FOR AS4/RIMR135 TOW WITH 80% FIBER VOLUME FRACTION

Property	Value	Unit
ρ^c	1.6720E-09	$\left[\frac{\text{tonnes}}{\text{mm}^3}\right]$
c_p^c	1.1978E+09	$\left[\frac{\text{mJ}}{\text{tonnes} \cdot ℃}\right]$
k_A^c	5.5130	$\left[\frac{\text{mW}}{\text{mm} \cdot ℃}\right]$
k_T^c	0.1556	$\left[\frac{\text{mW}}{\text{mm} \cdot ℃}\right]$

TABLE 4.—THERMOMECHANICAL PROPERTIES FOR AS4/RIMR135 TOW WITH 80% FIBER VOLUME FRACTION

Property	Value	Unit
E_A	185.3	[GPa]
E_T	10.74	[GPa]
ν_{12}	0.242	[-]
ν_{23}	0.3984	[-]
G_{12}	6.93	[GPa]
G_{23}	3.84	[GPa]
α_A	-0.334	$\left[10^{-6}/℃\right]$
α_T	27.82	$\left[10^{-6}/℃\right]$

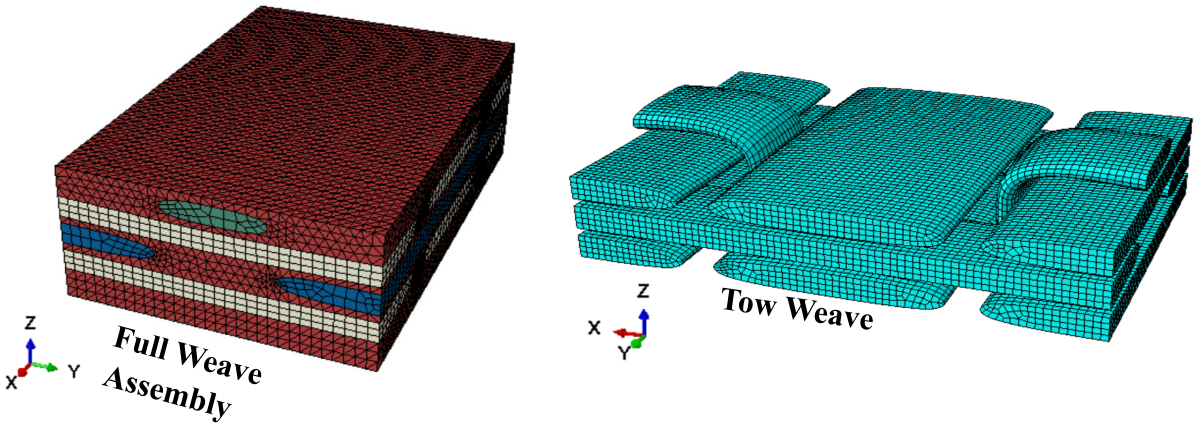

Figure 2.—Three-dimensional weave geometry meshed to 110,834 elements.

3.3 Boundary Conditions

The geometry was fixed on three sides, with the remaining three left free. The RUC is more representative of a flat 3D PMC panel in an oven, and thus the curing cycle for this model is applied to the outer *z*-faces only. Tow material properties remained constant to observe only the intertow matrix response to process modeling using small deformation assumptions. The deformation configuration along *x*, *y*, and *z* for both the RUC are shown in Figure 3. The reference frame used to represent a 3D PMC panel in an autoclave rotates the current reference frame clockwise by 90°.

The curing temperature profile and evolution of degree of cure with time are shown in Figure 4.

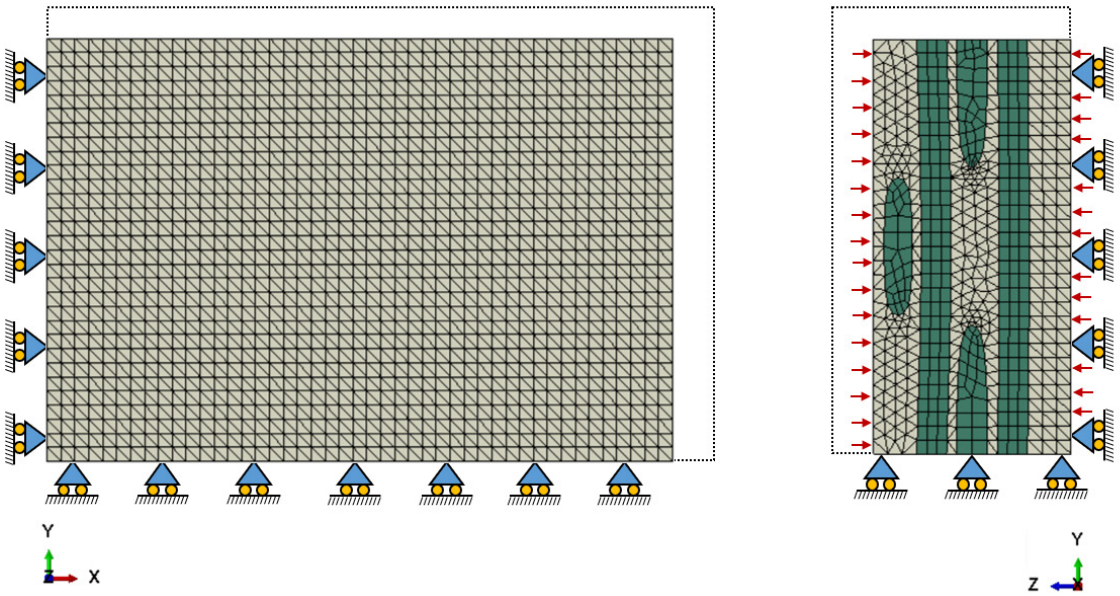

Figure 3.—RUC mechanical boundary constraints.

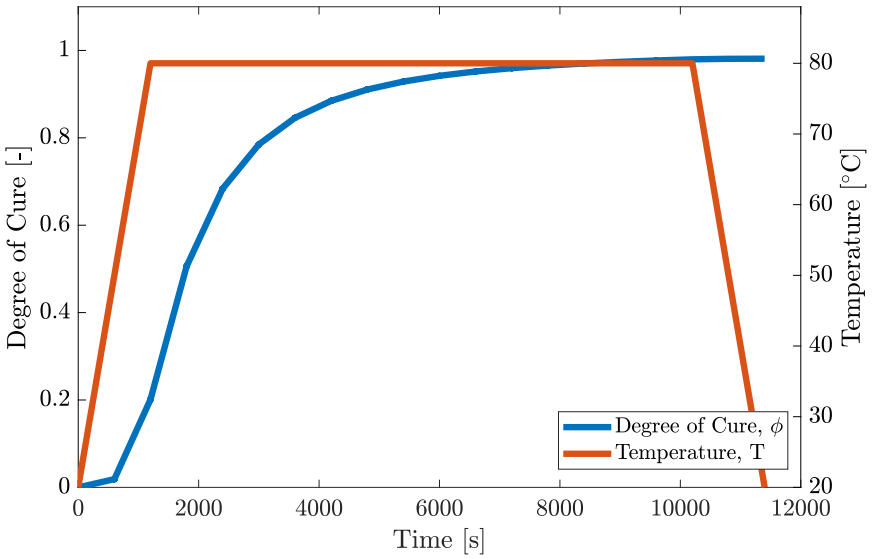

Figure 4.—Cure cycle.

4.0 Results and Discussion

The local residual maximum principal stress after curing is shown below in Figure 5 compared with an X-Ray-CT scan. A deformation scale factor of 8.6 was selected to visually represent the deformed model post-cure. The location of these stress concentrations coincides well with cracking observed in existing Micro-CT scan data (Ref. 30), thus supporting that the presence of the binder tow strongly contributes to residual stress buildup that is induced by the manufacturing process.

Overall, the bulk matrix material seems to have a relatively low stress during cure. However, during cure, the resin undergoes a significant reduction in strength. The higher stress concentrations observed in the 3D weave model serve as precursors for the failure observed in the X-Ray-CT scan. Experimental testing with the AS4/RIMR135 material system is required for a more quantitative analysis.

The stress evolution of the intertow matrix is quantified as a function of time and degree of cure in Figure 6. It can be seen from the t-dependent stress relation that the matrix is in a state of compression during the ramp-up phase and prior to gelation ($\phi_{gel} = 0.82$). The residual stress then increases gradually during the isothermal stage ($T = 80$ °C) and after gelation, during which chemical shrinkage dominates. The stress then increases again sharply during the thermal cooldown. When observing the ϕ-dependent stress relation, the process-induced stress increases drastically past gelation as the resin solidifies to retain stress at $\phi \approx 0.98$. Both plots show that the chemical shrinkage and thermal cooldown are driving factors for residual stress buildup within the matrix.

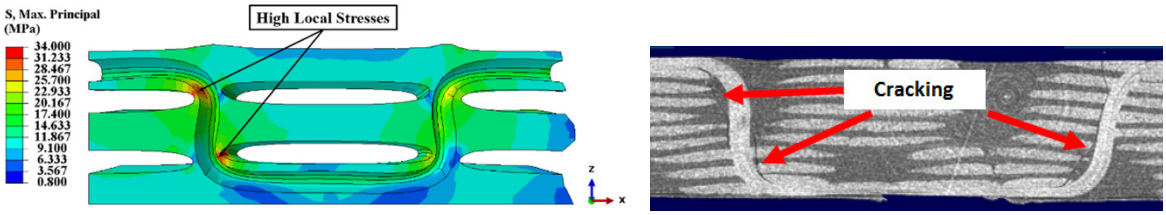

Figure 5.—High stress concentrations bordering binder tow compared with experimental evidence of microcracking in similar locations.

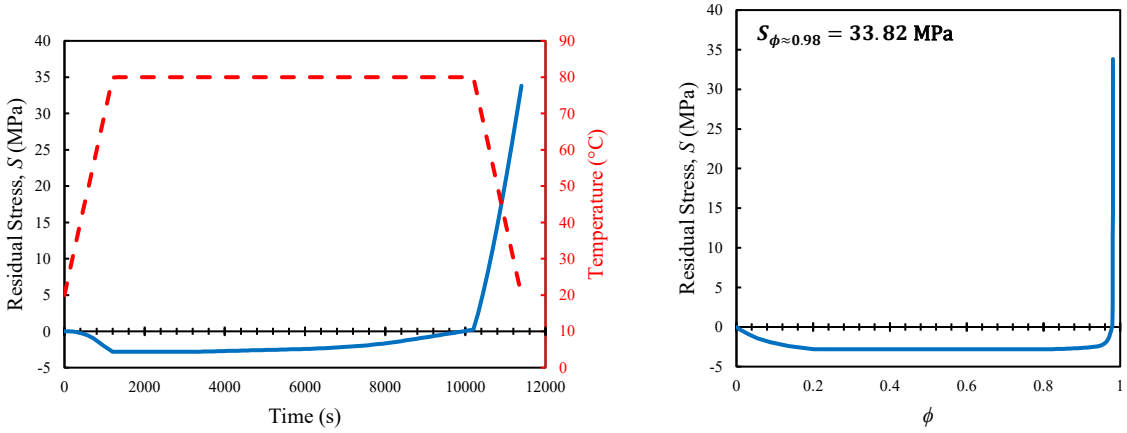

Figure 6.—Maximum principal stress of intertow matrix as a function of time and degree of cure ϕ.

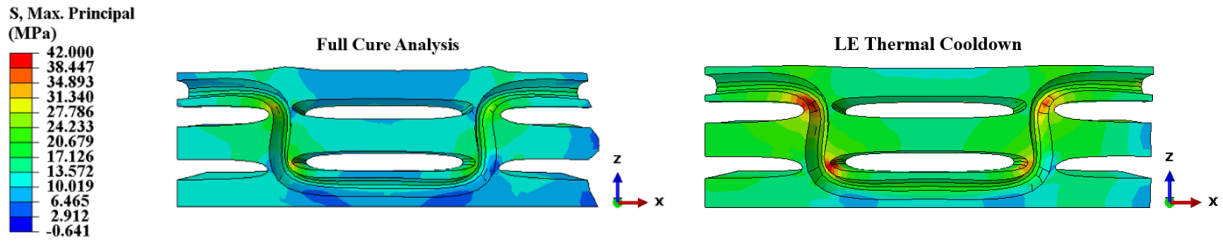

Figure 7.—End-of-cure residual stress comparison between full cure analysis and LE thermal cooldown.

In order to understand more how the curing of the bulk matrix resin process-induced stresses, a linear elastic (LE) thermal cooldown from the curing temperature (80 °C) to room temperature was conducted using constant material properties. The full cure of the intertow matrix and the thermal cooldown are compared under the same maximum principal stress scale, as shown in Figure 7.

It can be seen from Figure 7 that the LE thermal cooldown overestimates the state of stress. A thermal cooldown only accounts for the difference in the CTEs between the resin and the tow. Realistically, the stiffness of the resin material varies both thermally, temporally, as a function of the chemical reaction. At high temperatures, the resin stiffness is much lower than its value at the end of cure and room temperature. Furthermore, the resin CTE also varies with degree of cure. This property is orders of magnitude higher during the pre-gelation stage, during which the matrix is in a state of compression that is not accounted for in the LE thermal cooldown.

5.0 Conclusions

Prediction of processed-induced residual stresses was demonstrated within a repeating unit cell of an AS4/RIMR135 3D woven composite using the Arrhenius curing model and heat equation. Thermomechanical properties were approximated as a function of temperature and degree of cure using ROM and Bridging Model. Virtual curing of a 3D weave geometry was conducted to study residual stress evolution in the intertow matrix during processing. Stress concentrations were observed in areas bordering the binder tow that coincided with matrix microcracking in experimental testing data. A linear elastic thermal cooldown analysis was applied to the same mesoscale geometry to show that the state of stress can be overestimated when the thermal, temporal, and chemical evolutions of material properties are dismissed. These results are promising in that a low fidelity model provided accurate qualitative predictions. However, more insight is needed into the nonlinear response of the geometry at this scale. This framework will be further developed into an effective computational tool that will bridge the gap between the micro- to the macroscales. The tool will incorporate more sophisticated residual stress analysis models such an intratow matrix cure and a coupled intertow-intratow matrix cure. Damage modeling to predict crack initiation and propagation at various length scales such that failure mechanisms may be recognized. Refinement of the mesh and 3D weave geometry will be needed for damage modeling.

References

1. Jones, J.S., Polis, D.L., Rowles, R.R., and Segal, K.N. (2011). Comparative study of 3-dimensional woven joint architectures for composite spacecraft structures.
2. Bogdanovich, A.E. (2007, July). Advancements in manufacturing and applications of 3D woven preforms and composites. In *Proceeding of the 16th international conference on composites materials (ICCM-16)* (pp. 8–13).

3. Kazemianfar, B., Esmaeeli, M., and Nami, M.R. (2020). Experimental investigation on response and failure modes of 2D and 3D woven composites under low velocity impact. *Journal of Materials Science*, *55*(3), 1069–1091.
4. Saboktakin, A. (2019). 3D TEXTILE PREFORMS AND COMPOSITES FOR AIRCRAFT STRCUTURES: A REVIEW. *International Journal of Aviation, Aeronautics, and Aerospace*, *6*(1), 2.
5. Rudov-Clark, S.A., and Mouritz, A.P. (2008). Tensile fatigue properties of a 3D orthogonal woven composite. *Composites Part A: Applied Science and Manufacturing*, *39*(6), 1018–1024.
6. Clarke M. (2018) "3D Woven Textiles for Composite Applications". *PowerPoint Presentation*.
7. Yan, S., Zeng, X., and Long, A. (2018). Experimental assessment of the mechanical behaviour of 3D woven composite T-joints. *Composites part B: Engineering*, *154*, 108–113.
8. Mouritz, A.P., Bannister, M.K., Falzon, P.J., and Leong, K.H. (1999). Review of applications for advanced three-dimensional fibre textile composites. *Composites Part A: applied science and manufacturing*, *30*(12), 1445–1461.
9. Dadkhah, M.S., Cox, B.N., and Morris, W.L. (1995). Compression-compression fatigue of 3D woven composites. *Acta Metallurgica et Materialia*, *43*(12), 4235–4245.
10. Médeau, V., Laurin, F., Rannou, J., Hurmane, A., Quillent, H., and Lachaud, F. (2019). Robust characterization of crack propagation in 3D woven composites and evidences of size dependency. *Composite Structures*, *225*, 111175.
11. Huang, T., and Gong, Y. (2018). A multiscale analysis for predicting the elastic properties of 3D woven composites containing void defects. *Composite Structures*, *185*, 401–410.
12. D'Mello, R.J., Maiarù, M., and Waas, A.M. (2016). Virtual manufacturing of composite aerostructures. *The Aeronautical Journal*, *120*(1223), 61.
13. Guest, D.A., and Cairns, D.S. (2014). *Manufacturing process modeling for composite materials and structures, Sandia blade reliability collaborative* (No. SAND2014-0877). Sandia National Lab. (SNL-NM), Albuquerque, NM (United States); Montana State University, Bozeman, MT.
14. Gopal, A.K., Adali, S., and Verijenko, V.E. (2000). Optimal temperature profiles for minimum residual stress in the cure process of polymer composites. *Composite Structures*, *48*(1–3), 99–106.
15. Kim, K.S., and Hahn, H.T. (1989). Residual stress development during processing of graphite/epoxy composites. *Composites Science and Technology*, *36*(2), 121–132.
16. Heinrich, C., Aldridge, M., Wineman, A.S., Kieffer, J., Waas, A.M., and Shahwan, K.W. (2012). Generation of heat and stress during the cure of polymers used in fiber composites. *International Journal of Engineering Science*, *53*, 85–111.
17. Baran, I., Cinar, K., Ersoy, N., Akkerman, R., and Hattel, J.H. (2017). A review on the mechanical modeling of composite manufacturing processes. *Archives of computational methods in engineering*, *24*(2), 365–395.
18. Wang, Q., Li, T., Yang, X., Huang, Q., Wang, B., and Ren, M. (2020). Multiscale numerical and experimental investigation into the evolution of process-induced residual strain/stress in 3D woven composite. *Composites Part A: Applied Science and Manufacturing*, 105913.
19. Tsukrov, I., Bayraktar, H., Giovinazzo, M., Goering, J., Gross, T., Fruscello, M., and Martinsson, L. (2011). Finite element modeling to predict cure-induced microcracking in three-dimensional woven composites. *International journal of fracture*, *172*(2), 209–216.
20. Vasylevskyi, K., Buntrock, H., Gross, T., Drach, B., and Tsukrov, I. (2019, June). Numerical Evaluation of Reinforcement Morphology Contribution to Process-Induced Residual Stresses in 3D Woven Composites. In *Proceedings of NUMIFORM 2019: The 13th International Conference on Numerical Methods in Industrial Forming Processes*.

21. Gross, T.S., Jafari, H., Tsukrov, I., Bayraktar, H., and Goering, J. (2016). Curing cycle modification for RTM6 to reduce hydrostatic residual tensile stress in 3D woven composites. *Journal of Applied Polymer Science*, *133*(17).
22. Maiarù, M., D'Mello, R.J., and Waas, A.M. (2018). Characterization of intralaminar strengths of virtually cured polymer matrix composites. *Composites Part B: Engineering*, *149*, 285–295.
23. White, S.R., and Hahn, H.T. (1992). Process modeling of composite materials: residual stress development during cure. Part II. Experimental validation. *Journal of composite materials*, *26*(16), 2423–2453.
24. Zobeiry, N., Forghani, A., Li, C., Gordnian, K., Thorpe, R., Vaziri, R., and Poursartip, A. (2016). Multiscale characterization and representation of composite materials during processing. *Philosophical Transactions of the Royal Society A: Mathematical, Physical and Engineering Sciences*, *374*(2071), 20150278.
25. Dai, J., Xi, S., and Li, D. (2019). Numerical analysis of curing residual stress and deformation in thermosetting composite laminates with comparison between different constitutive models. *Materials*, *12*(4), 572.
26. Zobeiry, N. (2006). *Viscoelastic constitutive models for evaluation of residual stresses in thermoset composites during cure* (Doctoral dissertation, University of British Columbia).
27. Kamal, M.R. (1974). Thermoset characterization for moldability analysis. *Polymer Engineering and Science*, *14*(3), 231–239.
28. Wang, Y.C., and Huang, Z.M. (2015). A new approach to a bridging tensor. *Polymer Composites*, *36*(8), 1417–1431.
29. Enos, R. and Pineda, E.J. (2018) Developing Parametric Script for Generating Representative Volume Elements of 3D Woven Textiles. *NASA Student Intern Final Report*. NASA Glenn Research Center, Cleveland, OH.
30. Farrokh, B., Segal, K.N., Ricks, T.M., Miller, S.G., Rodini, B.T., and Sleight, D.S. (2019). Uniaxial Tensile Properties of AS4 3D Woven Composites with Four Different Resin Systems: Experimental Results and Analysis: Property Computations.